# PREDICTION OF POROSITY IN SLM PARTS USING A MARS STATISTICAL MODEL AND BAYESIAN INFERENCE

Tapia, G., Elwany, A. H.
Department of Industrial and Systems Engineering
Texas A&M University, College Station, TX
Email: gustapia06@tamu.edu, elwany@tamu.edu

REVIEWED

**Abstract**

Predictive models that establish a linkage between process parameters and part properties have been identified as a high priority research need in Additive Manufacturing. We work with a Multivariate Adaptive Regression Splines (MARS) statistical model to predict the porosity of parts produced using Selective Laser Melting (SLM) process as a function of process parameters. The proposed predictive model is validated through a case study on 17-4 PH stainless steel test coupons manufactured on a ProX 100 SLM system.

## 1 Introduction

Additive Manufacturing (AM) has evolved since its inception in the early 1980s to a $3.07 billion industry in 2013 with a compound annual growth rate of 32.3% over 2011-2013 [1]. Originally limited to producing visualization and functional prototypes from polymers to accelerate the product development cycle, metal-based AM technologies such as selective laser melting and electron beam melting are now capable of producing end-use parts from metallic materials and alloys including steels [2–7], titanium alloys [8–11], and nickel-based super alloys [12–15].

The technical barriers that still hamper the widespread adoption of metal-based AM are understood and identified in major roadmapping efforts [16–18]. These barriers include low process repeatability, part quality and properties, and lack of process standards. Some of these seem to have a common root: uncertainty and limited knowledge of the process, which causes variability in part properties and influences directly into part quality and performance [1]. This uncertainty is driven by the fact that most metal AM technologies involve complex physical transformations influenced by a large amount of process variables. For example, Selective Laser Melting (SLM) which is a class of laser-based Powder Bed Fusion (PBF) AM involves up to 30 variables [19, 20]. The development of models (both physics-based and statistical) are of paramount importance in order to better understand process-property relationships.

We develop a predictive model that links porosity (or density) of produced parts from a set of process parameters of the SLM process based on the Multivariate Adaptive Regression Splines (MARS) model introduced by Friedman [21]. MARS modeling is a flexible and easily interpretable method. It highlights relationships that are nearly additive or involve interactions of at most a few

variables, and then pinpoints important variables in the model [22]. Additionally, MARS can handle both continuous and categorical data and tend to have a good bias-variance trade-off, influenced by the flexibility or constraints given to its basis functions. Finally, predictions are calculated simply by evaluating the MARS model formula [23–25].

With the selected model, we aim to explain and predict the resulting porosity of the parts from a specific set of process parameters and we validate our methodology with a real-data case study from 17-4 PH stainless steel test samples built with a SLM machine.

The paper is organized as follows. We start by providing a review of relevant approaches for statistical modeling in Additive Manufacturing from the literature in Section 2, with emphasis to SLM and stainless steel. Next, in Section 3 we define and formulate the MARS model that we employ, followed in Section 4 by the Bayesian inference framework used to estimate model parameters. We then present and formulate how Prediction with the model is carried out in Section 5. Subsequently, we perform a case study, presented in Section 6, to establish validations of the proposed MARS model with real world data from 17-4PH stainless steel samples manufactured with SLM process. To finalize, Section 7 highlights milestones that need to be addressed and concludes the paper.

## 2 Literature Review

There are several studies on stainless steel with SLM that address microstructure, physical properties and manufacturability of parts. For instance, Cherry et al. [26] study the effect of process parameters on microstructural and physical properties, and Tolosa et al. [27] investigate mechanical properties of samples built with different orientations. Similarly, [28–30] analyze the microstructure and/or properties behavior of SLM-fabricated stainless steel parts.

SLM depends on a set of process variables that affect the properties of manufactured parts, however there has not been any agreement or formal discussion yet about standardizing this set of all influencing process parameters. The common trend in the literature that the parameters that possess the highest influence on the properties of SLM parts include: laser power, laser scanning speed, powder layer thickness, and hatch distance (the distance between two successive passes of the laser beam in the same layer) [31–35]. Researchers have investigated the influence of process parameters on end-part properties following systematic methodologies, with tools such as experimental design, ANOVA and Taguchi's method (see for example [36–40]).

In this study, we do use a systematic methodology and construct a predictive model based on the popular MARS statistical model, in order to predict the porosity of SLM-manufactured samples.

MARS statistical model was originally developed by Friedman [21] in 1991. It has been widely used for several applications such as ecology, economy, biology and sociology, however, to the extent of our knowledge, it has never been employed in any investigation regarding AM.

## 3 MARS Statistical Model

Before we start the mathematical formulation of the model, we define its objective and set inputs and outputs. Our goal is to investigate the behavior of part porosity as a function of SLM process parameters. From Section 2, 4 process parameters were identified as to have the most significant impact on part properties. We focus on Laser Power ($P$) and Scanning Speed ($v$) for input variables in this work. However, we can extend the model to include more than 2 variables in the analysis, which would help to identify significant variables in the process – one of the strengths of MARS model.

We define part porosity as the model response $Y$, and $\boldsymbol{\mathcal{S}} \in \mathbb{D} \subset \mathbb{R}^2$ as a location inside a bounded study region $\mathbb{D}$ in the two-dimensional $P - v$ space. Location $\boldsymbol{\mathcal{S}}$ is defined by the pair $(\mathcal{S}_P, \mathcal{S}_v)$, with $\mathcal{S}_P$ and $\mathcal{S}_v$ representing values of the laser power and scanning speed, respectively. Finally, we define function $h\colon \mathbb{R}^2 \mapsto \mathbb{R}^p$ to be the mapping from a location $\boldsymbol{\mathcal{S}}$ to the vector of predictors $\mathbf{X}$ containing $p$ elements (note that most of the time $\mathbf{X} = \boldsymbol{\mathcal{S}}$).

The regression problem is to model the dependence of a response variable $Y$ (generally noisy) on a set of $p$ predictor variables $\mathbf{X} = (x_1, \ldots, x_p)$, by the relationship

$$Y = f(\mathbf{X}) + \epsilon \tag{1}$$

where $f(\cdot)$ is an unknown function and $\epsilon$ is the random error component, assumed as zero-mean Gaussian distribution with variance $\sigma^2$.

The model estimates the function $f$ with a function $g$ explained by

$$g(\mathbf{X}) = \beta_0 + \sum_{i=1}^{k} \beta_i B_i(\mathbf{X}) \tag{2}$$

where $k$ is the total number of basis functions in the model, $\boldsymbol{\beta} = (\beta_0, \ldots, \beta_k)^\top$ is the set of coefficients corresponding to basis functions set $\mathbf{B} = (1, B_1, \ldots, B_k)$. It should be noted that the model always includes an intercept term $\beta_0$.

The ith basis function $B_i(\mathbf{X})$ is given by

$$B_i(\mathbf{X}) = \prod_{j=1}^{J_i} \left[ s_{i,j} \left( x_{w_{i,j}} - t_{i,j} \right) \right]_+^{q_i} \tag{3}$$

with $[\cdot]_+ = \max(0, \cdot)$, $J_i$ is the degree of interaction of basis $B_i$, $s_{i,j}$ are sign indicators taking values $\{\pm 1\}$, $q_i$ is the order of basis $B_i$, $w_{i,j}$ give the index of the predictor variable which have an associated knot, $t_{i,j}$ are known as knot points and give the position of the splits. It should be noted that $\{w_{i,1}, \ldots, w_{i,J_i}\}$ are constrained to be all distinct for each basis $B_i$, so each predictor $x_b$ $(b = \{1, \ldots, p\})$ is present only once or not present at all. Furthermore, knot points $t_{i,j}$ only take values present in $\mathbf{X}$ of the corresponding predictor $x_{w_{i,j}}$. The reader should refer to [21, 22, 41] for a more detailed definition of the model.

From this parameterization, the model depends on a set of model parameters

$$\boldsymbol{\Omega} = \left\{ \boldsymbol{\beta}, k, \boldsymbol{\theta}, \sigma^2 \right\} \tag{4}$$

where $\boldsymbol{\theta} = \{\boldsymbol{\mathcal{B}}_1, \ldots, \boldsymbol{\mathcal{B}}_k\}$, and $\boldsymbol{\mathcal{B}}_i$ is the parameter vector for a single basis $B_i$,

$$\boldsymbol{\mathcal{B}}_i = \{J_i, q_i, s_{i,1}, \ldots, s_{i,J_i}, t_{i,1}, \ldots, t_{i,J_i}, w_{i,1}, \ldots, w_{i,J_i}\}$$

The original regression method developed and published by Friedman [21] calculates the model and its parameters via two phases: a forward phase which repeatedly adds basis function in pairs to the model, same function but different sign values $s_{i,j}$, and finds the basis functions that gives the maximum reduction in sum-of-squares residual error; and a backward pass which removes basis that overfit the model until it finds the best submodel [21]. However, we utilize a Bayesian inference framework to estimate the value for all model parameters.

## 4 Bayesian Inference Framework

Application of Bayesian analysis to a MARS model has been previously presented by Denison et al. [22], Denison [41]. We have relied in their research findings and calculations, to make modifications according to our application.

Within this analysis, we treat the model parameters $\boldsymbol{\Omega}$ as random variables that follow some joint probability distribution, instead of being constant values. Therefore, after observing experimental data $\mathcal{D}$ (also random in nature), following Bayes' Theorem, we have

$$p\left(\boldsymbol{\Omega}|\mathcal{D}\right) \propto p\left(\mathcal{D}|\boldsymbol{\Omega}\right) p\left(\boldsymbol{\Omega}\right) \tag{5}$$

where $p\left(\mathcal{D}|\boldsymbol{\Omega}\right)$ is the likelihood, $p\left(\boldsymbol{\Omega}\right)$ is the prior distribution that explains some degree of belief that one may have about the parameters before observing the data, and $p\left(\boldsymbol{\Omega}|\mathcal{D}\right)$ is the posterior distribution of the parameters which explains what the parameters might be, given the observed data.

In the next subsections, we describe the nature or assumptions that we made for each one of these probability distributions.

### 4.1 Likelihood

We define the experimental data set with *n* observations as $\mathcal{D} = \{\mathbf{Y}, \mathbb{X}\}$, with $\mathbf{Y} = (Y_1, \ldots, Y_n)^\top$ and $\mathbb{X} = (\mathbf{X}_1, \ldots, \mathbf{X}_n)$.

The new notation turns the model of equations (1) and (2) to

$$\mathbf{Y} = \mathbf{B}\boldsymbol{\beta} + \boldsymbol{\epsilon}$$

and because of the normality assumption, the likelihood distribution is

$$p\left(\mathcal{D}|\boldsymbol{\Omega}\right) \sim \text{MVN}\left(\mathbf{B}\boldsymbol{\beta}, \sigma^2\mathbf{I}_n\right) \tag{6}$$

where $\mathbf{I}_n$ is the identity matrix of size *n*.

### 4.2 Priors

Our task now is to select the prior distributions that will help calculate the posterior from equation (5). Because prior probabilities specify some previous knowledge about a certain parameter, we need to choose these prior distributions careful enough so we don't give false information that can influence in the estimation and yield wrong results.

First of all, we will assume that all parameters are independent of one another, that is

$$p(\boldsymbol{\Omega}) = p(\boldsymbol{\beta})\, p(k)\, p(\boldsymbol{\theta})\, p\left(\sigma^2\right) \tag{7}$$

Second, because we don't really have any strong prior information about any parameter, we choose non-informative distributions for the parameters. Furthermore, we choose to use conjugate prior distributions for some parameters to simplify estimation and calculations of the parameters [41–43].

For the set of coefficients $\boldsymbol{\beta}$, we set a Normal conjugate prior

$$p\left(\boldsymbol{\beta}\middle|\sigma^2, v, \boldsymbol{\theta}\right) \sim \text{MVN}\left(\mathbf{m}, \sigma^2\mathbf{V}\right)$$

where $\mathbf{m}$ is a known prior mean vector, and $\mathbf{V} = \text{diag}\,(\infty, v, \ldots, v)$, a $k+1$ diagonal matrix. This matrix adds a new hyperparameter $v$ to the model; it is the inverse of a precision in the distribution and helps to robustify the estimation. Additionally, the infinity value used in the first value in $\mathbf{V}$ implies to have always an intercept term [41].

Next, for variances parameters $\sigma^2$ and $v$, we select the Inverse Gamma conjugate prior

$$\begin{aligned} p\left(\sigma^2\right) &\sim \text{IG}\,(a, b) \\ p(v) &\sim \text{IG}\,(\delta_1, \delta_2) \end{aligned}$$

For the rest of parameters, we use uniform non-informative priors as we don't have any previous idea of their values, nor there is a conjugate prior distribution,

$$\begin{aligned} p(k) &\sim \text{D. Unif}\,(1, k_{\text{max}}) \\ p(q_i) &\sim \text{D. Unif}\,(0, q_{\text{max}}) \\ p(J_i) &\sim \text{D. Unif}\,(1, J_{\text{max}}) \\ p(s_{i,j}) &\sim \text{D. Unif}\,\{-1, 1\} \\ p(w_{i,j}) &\sim \text{D. Unif}\left\{1, \ldots, p \setminus \{w_{i,r}\}_{r=1:j-1}\right\} \\ p(t_{i,j}) &\sim \text{D. Unif}\left\{x^{(r)}_{w_{i,j}}\right\}_{r=1:n} \end{aligned}$$

From these prior distributions, all of them are straight forward to follow except for the last two. Distribution for $w_{i,j}$ tells us what we defined before: these variables are to be different from one another among each basis $i$. In the case for $t_{i,j}$, splits are only permissible at the marginal predictor observed values.

### 4.3 Posterior

From the formulation of likelihood and priors, we should be able to follow equation (5) to calculate the posterior distribution. However, this is not the case as an explicit formula for this distribution might not even exist. To face this problem, we can rely on Markov Chain Monte Carlo (MCMC) methods, specifically Gibbs sampler and Reversible-Jump Metropolis-Hastings algorithm [41], which will allow us to draw samples from posterior distribution and perform statistical inference of parameters afterwards.

Because we are using conjugate priors for $\boldsymbol{\beta}, \sigma^2, v$, we are able to explicitly calculate each posterior full conditional distribution and employ Gibbs sampler to draw samples from those distributions. However, we do not have any explicit formula for the rest of the parameters. Furthermore, we see that parameter $k$ controls the dimensionality of the parameter set $\boldsymbol{\Omega}$; then for each iteration, we are sampling a new value of $k$, and consequently, the size of the parameter set $\boldsymbol{\Omega}$ is changing.

To tackle these two problems, we resort on the Reversible-Jump algorithm, which works with three different steps, selected randomly at each MCMC iteration:

- *Birth:* increase $k$ by 1, therefore propose to add a new basis function.
- *Death:* decrease $k$ by 1, therefore propose to remove a randomly chosen basis function from the present model.
- *Move:* Keep the same value of $k$, therefore modify the parameters of a randomly chosen basis function by sampling them again.

The interested reader should refer to [41, 42, 44, 45] about details of MCMC algorithms, conjugate priors and posteriors, and full conditional distributions.

## 5 Prediction

Prediction for the MARS model is straightforward. After running the MCMC sampling for $N$ iterations in the previous step, we have generated each sample point $\boldsymbol{\Omega}^{(i)}$ from the distribution $p(\boldsymbol{\Omega}|\mathcal{D})$. Consequently, prediction over the model is done by evaluating the following equation, where the expected porosity $Y_0$ at a new input $\mathbf{X}_0$ will be

$$\mathrm{E}\left[Y_0|\mathbf{X}_0, \mathcal{D}\right] \approx \frac{1}{N}\sum_{i=1}^{N} \mathrm{E}\left[Y_0\middle|\mathbf{X}_0, \mathcal{D}, \boldsymbol{\Omega}^{(i)}\right] \tag{8}$$

where $\mathrm{E}\left[Y_0\middle|\mathbf{X}_0, \mathcal{D}, \boldsymbol{\Omega}^{(i)}\right] = g\left(\mathbf{X}_0\right)\middle|\boldsymbol{\Omega}^{(i)}$.

Similarly, the prediction standard error is calculated among all sample points, that is

$$\mathrm{SE}\left[Y_0|\mathbf{X}_0, \mathcal{D}\right] \approx \sqrt{\mathrm{Var}\left[g\left(\mathbf{X}_0\right)\middle|\boldsymbol{\Omega}^{(i)}\right]_{i=1:N}} \tag{9}$$

Table 1: Chemical composition of the 17-4 PH stainless steel powder

| **Element** | Fe | Cr | Ni | HC Cu |
|---|---|---|---|---|
| **Concentration (%)** | 70 – 80 | 10 – 25 | 1.0 – 10 | 1.0 – 10 |

## 6 Case Study

The model formulated in Section 3, and estimated in Sections 4 and 5, is demonstrated through an experimental dataset collected at the Laboratory of Additive Manufacturing in the Department of Industrial and Systems Engineering at Texas A&M University. The experiment consisted on measuring the porosity of various test parts built by SLM process from 17-4 PH stainless steel by varying the process parameters.

### 6.1 Data Collection

For the case study, we selected a simple cube geometry for the test parts, with size of $10 \times 10 \times 10$ mm. They were produced on a 3D Systems ProX100 machine that employs the SLM process. The system is equipped with a laser beam having a Gaussian profile and wavelength at $\lambda = 1070$ nm, beam spot size of approximately $70$ $\mu$m-diameter, and a maximum power of $50$ W.

The material used for the experiments was 17-4 PH stainless steel powder from 3D Systems, produced by gas atomization and with chemical composition shown in Table 1. The particle size distribution is $10\,\mu\text{m} < \text{D50} < 13.5\,\mu\text{m}$ and $\text{D80} < 22\,\mu\text{m}$, where D$xx$ means $xx$% of the particles in a batch of powder. The coupons were built on a substrate made of 430F Stainless Steel and Argon was used as inert protective gas during manufacturing.

As previously explained, we selected Power Laser ($P$) and Scanning Speed ($v$) to be the inputs to the model. Consequently, we have kept constant the other two important parameters, hatch distance at $50\,\mu$m and layer thickness at $30\,\mu$m. These values were chosen following the recommended settings for material and machine from the manufacturer.

A 10-by-10 uniformly spaced grid on the considered $P-v$ space was devised with the following configuration:

- Laser Power: from $P = 41$ to $50$ W, in $1$ W steps.
- Laser Scanning Speed: from $v = 287.5$ to $400$ mm/s, in $12.5$ mm/s steps.

These values were also selected following manufacturer optimal settings, machine capabilities and values from literature.

Figure 1 shows 10 as-built test coupons prior to using electrical discharge machining (EDM) to cut them from the substrate. The porosity (or density) of the test parts were then measured using the Archimedes' principle according to the standard ASTM B962-14 [46].

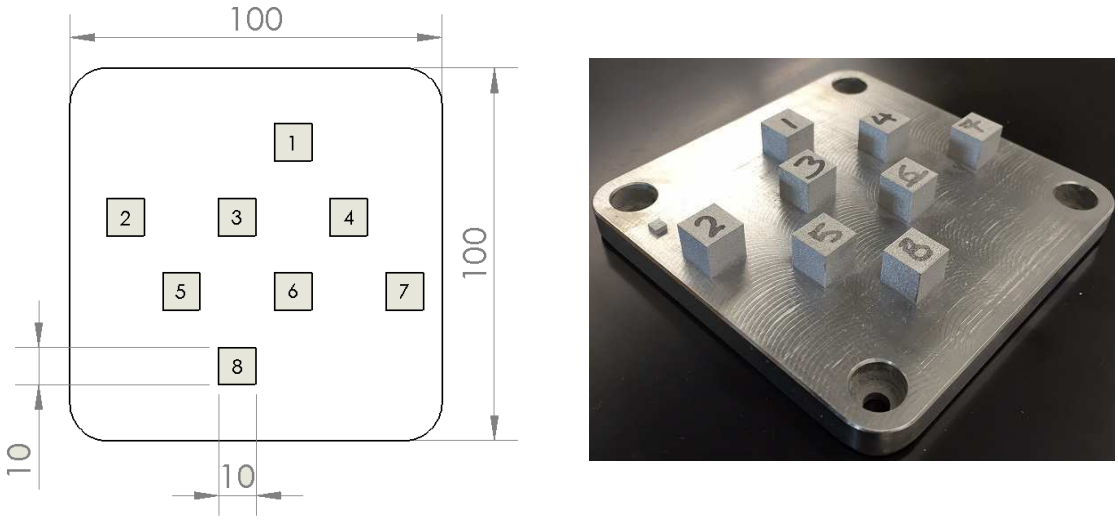


Figure 1: Drawing (in mm) and As-built test coupons

### 6.2 Preliminary data analysis

From the experimental plan explained in the last subsection, 42 test cubes were produced each one having a different $P - v$ combination and representing a data point on the defined spatial grid. The measured porosity for these parts is shown in Figure 2a. Spatial behavior can be observed in the figure, with most of high values located in the top left corner and low porosities in the bottom right. Additionally, to verify the normality assumption made in equation (6), we present a Normal Q-Q plot in Figure 2b. The plot shows that the data follows very close the normality line, consequently, corroborating our assumption to be valid.

### 6.3 Estimation of model parameters

As mentioned in Section 4, we selected non-informative priors for all of the parameters, as well as conjugate prior to a few of them. Selection of hyperparameters was based on the need for the model to be able to explain additive and interaction behavior among variables, while keeping it simple and avoiding high order complexities. The following specific priors were used:

$$
\begin{aligned}
p\left(\boldsymbol{\beta}\middle|\sigma^2, v, \boldsymbol{\theta}\right) &\sim \text{MVN}\left(\mathbf{0}, \sigma^2\mathbf{V}\right) \\
p\left(\sigma^2\right) &\sim \text{IG}\left(1, 0.1\right) \\
p\left(v\right) &\sim \text{IG}\left(1, 0.05\right) \\
p\left(k\right) &\sim \text{D. Unif}\left(1, 500\right) \\
p\left(q_i\right) &\sim \text{D. Unif}\left(0, 2\right) \\
p\left(J_i\right) &\sim \text{D. Unif}\left(0, 2\right)
\end{aligned}
$$

Priors for $s_{i,j}, w_{i,j}, t_{i,j}$ were already defined in Section 4 and didn't need any further specification. We can analyze the different choices of priors made: the maximum number of basis functions

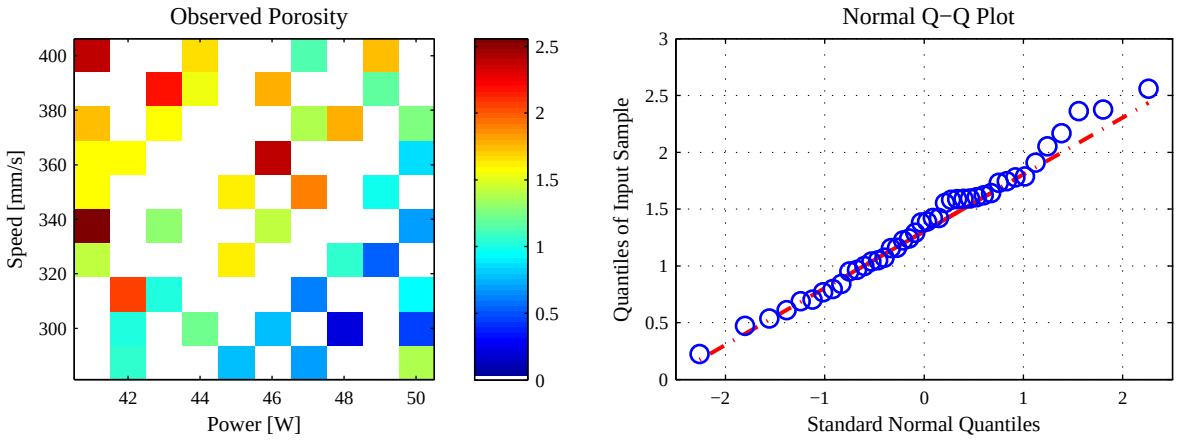


Figure 2: Initial analysis of the data. **a)** Spatial behavior of the observations across the grid. A white value means no observation in that location. **b)** Normal Q-Q plot for the initial data.

that we allow in the model is $k_{max} = 500$, which should be enough to represent the process; we set the maximum order of basis function to be of second order, $q_{max} = 2$, to avoid high-order complexities; and the maximum number of interaction is $J_{max} = 2$, which means full interaction between the two covariates (it can't go above that as each covariate can only appear at most once for each basis). The choice for $\boldsymbol{\beta}$ prior is also straightforward, we set the prior mean to be zero to reflect ignorance about the sign of the coefficients as we don't know anything beforehand.

The choices for the variance priors $(\sigma^2, v)$ are not as easy interpretable as the other parameters. First of all, we have to remark some facts about the Inverse Gamma distribution; for the parameterization that we use (i.e. IG $(\alpha, \beta)$), the mean is $\frac{\beta}{\alpha-1}$ with $\alpha > 1$, variance is $\frac{\beta^2}{(\alpha-1)^2(\alpha-2)}$ with $\alpha > 2$, and mode is $\frac{\beta}{\alpha+1}$. From these quantities, we can now say that the values used for priors have been set to not have a mean nor a variance (no information of the parameters a priori), however we set a small value for the mode, making sure to have a proper distribution [41].

Once all the data has been collected and priors have been set, we run the MCMC sampler in two phases; first we let it stabilize for 50,000 iterations as burn-in period, and record the next 100,000 iterations as sample points. Consequently, we can proceed on to the next step to compute predictions over unobserved locations.

### 6.4 Prediction of porosity

In this step, we make predictions about the response of the model following equations (8) and (9). The results for expected porosity and standard prediction error over the same study region of the initial observations are shown in Figures 3a and 3b respectively. From these colormaps, we see a very defined pattern of how porosity behaves across the study domain. Relative high values of porosity are predicted on the top left corner where combinations of low power and high speed happen. Conversely, parts less porous are predicted to happen at a combination of high power and low speed.

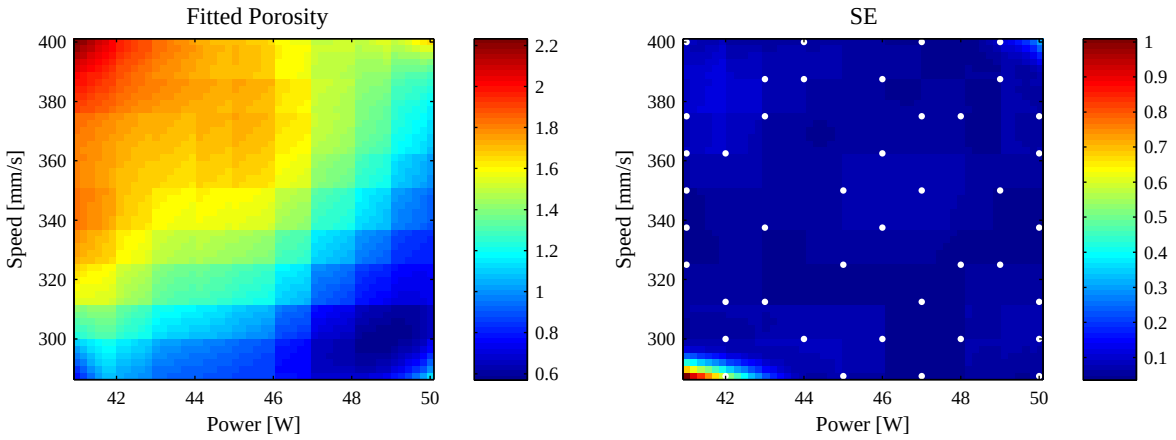


Figure 3: Prediction results in the defined spatial range. **a)** Fitted (predicted) porosity. **b)** Prediction Standard Error for the predicted values. The white dots represent the locations of the initially observed data points.

These results do make sense because as a laser beam scanning on the material with high power at a slow pace, means that more energy is being transferred to the material, and in consequence, the material particles are more probable to melt and bond between each other, creating a less porous and more uniform part. This also can be explained through the widely known energy density equation in SLM, $E = {}^{P}/_{v \cdot d \cdot t}$, where $E$ is the energy density and a function of the laser power $P$, scanning speed $v$, hatch distance $d$, and layer thickness $t$. This equation also explains the idea behind the results obtained through the model (low porosities expected at high power and low speeds).

The prediction standard error plot of Figure 3b describes a uniformly low error across the space except for the lower left corner. This low error value means that the model is consistent and predicting similar values along each iteration, which may imply good convergence of the parameters in the MCMC run.

### 6.5 Model Validation

To verify the model, we run comparisons between the predicted values and actual observations to analyze how good the model performance is, and present them in Figure 4. An ideal model would be the one where the predictions are exactly equal to the observations, and thus would result on points following the red line. We understand that no model is ideal but we want to be close to it. We can see that the model predictions follow closely the ideal line, therefore we can agree that the model is a very good approximation to the real process.

To analyze it from a statistical standpoint, we calculated the standard deviation (or error) of the predictions compared the experimental observations:

$$\mathrm{SD}_{\mathrm{pred}} = \sqrt{\frac{\sum_i \left(Y_{\mathrm{obs},i} - Y_{\mathrm{pred},i}\right)^2}{n}} = 0.2722$$

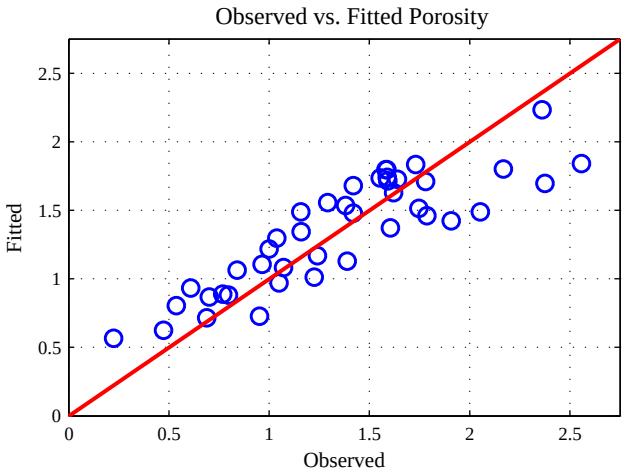


Figure 4: Comparison of the observed and predicted values of porosity

and this low value confirms that the model explains closely the physical process.

## 7 Conclusions

We develop a Multivariate Adaptive Regression Splines (MARS) statistical model to make prediction of porosity in parts produced with SLM as a function of process parameters – specifically laser power and scanning speed. A Bayesian estimation framework was used to estimate the model parameters. The proposed model is applied in a real industrial-like case study to explain the resulting porosity of parts made of 17-4 PH stainless steel by the SLM process, with the objective to make predictions and find combinations of inputs that yield parts with low porosity.

Extensions to this study include adding more variables to the model, and making inference about the ones that have more significant influence on the part properties. Examples of these additional variables are process-related variables such as hatch distance, layer thickness, and oxygen content, or material-related variables such as powder particle size and morphology. It should be noted that the predictive statistical model developed in this study could also be used in other AM technologies such as EBM or LENS.

As this model is purely data driven, future plans for this ongoing research include work with materials and physics-based models which will provide more knowledge into the statistics and help improve predictions.

## References

[1] Terry Wohlers. *Wohlers Report 2013: Additive Manufacturing and 3D Printing State of the Industry–Annual Worldwide Progress Report, Wohlers Associates*. Fort Collins Inc., 2013.

[2] H Khalid Rafi, Deepankar Pal, Nachiket Patil, Thomas L Starr, and Brent E Stucker. Microstructure and mechanical behavior of 17-4 precipitation hardenable steel processed by se-

lective laser melting. *Journal of Materials Engineering and Performance*, 23(12):4421–4428, 2014.

[3] Lawrence E Murr, Sara M Gaytan, Diana A Ramirez, Edwin Martinez, Jennifer Hernandez, Krista N Amato, Patrick W Shindo, Francisco R Medina, and Ryan B Wicker. Metal fabrication by additive manufacturing using laser and electron beam melting technologies. *Journal of Materials Science & Technology*, 28(1):1–14, 2012.

[4] Lawrence E Murr, Edwin Martinez, Jennifer Hernandez, Shane Collins, Krista N Amato, Sara M Gaytan, and Patrick W Shindo. Microstructures and properties of 17-4 ph stainless steel fabricated by selective laser melting. *Journal of Materials Research and Technology*, 1 (3):167–177, 2012.

[5] M Averyanova, Ph Bertrand, and B Verquin. Studying the influence of initial powder characteristics on the properties of final parts manufactured by the selective laser melting technology: A detailed study on the influence of the initial properties of various martensitic stainless steel powders on the final microstructures and mechanical properties of parts manufactured using an optimized slm process is reported in this paper. *Virtual and Physical Prototyping*, 6(4): 215–223, 2011.

[6] M Averyanova, E Cicala, Ph Bertrand, and Dominique Grevey. Experimental design approach to optimize selective laser melting of martensitic 17-4 ph powder: part i-single laser tracks and first layer. *Rapid Prototyping Journal*, 18(1):28–37, 2012.

[7] A Riemer, S Leuders, M Thöne, HA Richard, T Tröster, and T Niendorf. On the fatigue crack growth behavior in 316l stainless steel manufactured by selective laser melting. *Engineering Fracture Mechanics*, 120:15–25, 2014.

[8] Bo Song, Shujuan Dong, Baicheng Zhang, Hanlin Liao, and Christian Coddet. Effects of processing parameters on microstructure and mechanical property of selective laser melted ti6al4v. *Materials & Design*, 35:120–125, 2012.

[9] Dongdong Gu, Yves-Christian Hagedorn, Wilhelm Meiners, Guangbin Meng, Rui João Santos Batista, Konrad Wissenbach, and Reinhart Poprawe. Densification behavior, microstructure evolution, and wear performance of selective laser melting processed commercially pure titanium. *Acta Materialia*, 60(9):3849–3860, 2012.

[10] S Leuders, M Thöne, A Riemer, T Niendorf, T Tröster, HA Richard, and HJ Maier. On the mechanical behaviour of titanium alloy tial6v4 manufactured by selective laser melting: Fatigue resistance and crack growth performance. *International Journal of Fatigue*, 48:300–307, 2013.

[11] Bey Vrancken, Lore Thijs, Jean-Pierre Kruth, and Jan Van Humbeeck. Heat treatment of ti6al4v produced by selective laser melting: Microstructure and mechanical properties. *Journal of Alloys and Compounds*, 541:177–185, 2012.

[12] Zemin Wang, Kai Guan, Ming Gao, Xiangyou Li, Xiaofeng Chen, and Xiaoyan Zeng. The microstructure and mechanical properties of deposited-in718 by selective laser melting. *Journal of Alloys and Compounds*, 513:518–523, 2012.

[13] P Kanagarajah, F Brenne, T Niendorf, and HJ Maier. Inconel 939 processed by selective laser melting: Effect of microstructure and temperature on the mechanical properties under static and cyclic loading. *Materials Science and Engineering: A*, 588:188–195, 2013.

[14] KN Amato, SM Gaytan, LE Murr, E Martinez, PW Shindo, J Hernandez, S Collins, and F Medina. Microstructures and mechanical behavior of inconel 718 fabricated by selective laser melting. *Acta Materialia*, 60(5):2229–2239, 2012.

[15] Qingbo Jia and Dongdong Gu. Selective laser melting additive manufacturing of inconel 718 superalloy parts: Densification, microstructure and properties. *Journal of Alloys and Compounds*, 585:713–721, 2014.

[16] David L Bourell, Ming C Leu, and David W Rosen. Roadmap for additive manufacturing: identifying the future of freeform processing. *The University of Texas at Austin, Austin, TX*, 2009.

[17] National Institute of Standards and Technology (NIST). Measurement science roadmap for metal-based additive manufacturing, 2013. Online; Accessed 10 June, 2015.

[18] William E Frazier. Direct digital manufacturing of metallic components: vision and roadmap. *Direct Digital Manufacturing of Metallic Components: Affordable, Durable, and Structurally Efficient Airframes, at Solomons Island, MD*, 2010.

[19] Mukesh Agarwala, David Bourell, Joseph Beaman, Harris Marcus, and Joel Barlow. Direct selective laser sintering of metals. *Rapid Prototyping Journal*, 1(1):26–36, 1995.

[20] Sanjay Kumar. Selective laser sintering: a qualitative and objective approach. *JOM*, 55(10): 43–47, 2003.

[21] Jerome H Friedman. Multivariate adaptive regression splines. *The Annals of Statistics*, 19 (1):1–67, 1991.

[22] David GT Denison, Bani K Mallick, and Adrian FM Smith. Bayesian MARS. *Statistics and Computing*, 8(4):337–346, 1998.

[23] Jerome H Friedman. Estimating functions of mixed ordinal and categorical variables using adaptive splines. Technical report, DTIC Document, 1991.

[24] Jerome H Friedman. Fast MARS. Technical report, Laboratory for Computational Statistics, Stanford University, 1993.

[25] Jerome H Friedman and Charles B Roosen. An introduction to multivariate adaptive regression splines. *Statistical Methods in Medical Research*, 4(3):197–217, 1995.

[26] JA Cherry, HM Davies, S Mehmood, NP Lavery, SGR Brown, and J Sienz. Investigation into the effect of process parameters on microstructural and physical properties of 316L stainless steel parts by selective laser melting. *The International Journal of Advanced Manufacturing Technology*, 76(5-8):869–879, 2014.

[27] Itziar Tolosa, Fermín Garciandía, Fidel Zubiri, Fidel Zapirain, and Aritz Esnaola. Study of mechanical properties of AISI 316 stainless steel processed by selective laser melting, following different manufacturing strategies. *The International Journal of Advanced Manufacturing Technology*, 51(5-8):639–647, 2010.

[28] Luca Facchini, Nério Vicente, Ivan Lonardelli, Emanuele Magalini, Pierfrancesco Robotti, and Alberto Molinari. Metastable austenite in 17–4 precipitation-hardening stainless steel produced by selective laser melting. *Advanced Engineering Materials*, 12(3):184–188, 2010.

[29] Sanjay Kumar and J-P Kruth. Wear performance of SLS/SLM materials. *Advanced Engineering Materials*, 10(8):750–753, 2008.

[30] M Averyanova, Ph Bertrand, and B Verquin. Studying the influence of initial powder characteristics on the properties of final parts manufactured by the selective laser melting technology: A detailed study on the influence of the initial properties of various martensitic stainless steel powders on the final microstructures and mechanical properties of parts manufactured using an optimized slm process is reported in this paper. *Virtual and Physical Prototyping*, 6(4): 215–223, 2011.

[31] M Averyanova, E Cicala, Ph Bertrand, and Dominique Grevey. Experimental design approach to optimize selective laser melting of martensitic 17-4 PH powder: part I-single laser tracks and first layer. *Rapid Prototyping Journal*, 18(1):28–37, 2012.

[32] AN Chatterjee, Sanjay Kumar, P Saha, PK Mishra, and A Roy Choudhury. An experimental design approach to selective laser sintering of low carbon steel. *Journal of Materials Processing Technology*, 136(1):151–157, 2003.

[33] Prashant K Jain, Pulak M Pandey, and PVM Rao. Experimental investigations for improving part strength in selective laser sintering. *Virtual and Physical Prototyping*, 3(3):177–188, 2008.

[34] Jean-Pierre Kruth, Sanjay Kumar, and Jonas Van Vaerenbergh. Study of laser-sinterability of ferro-based powders. *Rapid Prototyping Journal*, 11(5):287–292, 2005.

[35] J-P Kruth and Sanjay Kumar. Statistical analysis of experimental parameters in selective laser sintering. *Advanced Engineering Materials*, 7(8):750–755, 2005.

[36] S Dingal, TR Pradhan, JK Sarin Sundar, A Roy Choudhury, and SK Roy. The application of Taguchi's method in the experimental investigation of the laser sintering process. *The International Journal of Advanced Manufacturing Technology*, 38(9-10):904–914, 2008.

[37] A Simchi. Direct laser sintering of metal powders: Mechanism, kinetics and microstructural features. *Materials Science and Engineering: A*, 428(1):148–158, 2006.

[38] AB Spierings, G Levy, and Konrad Wegener. *Designing material properties locally with Additive Manufacturing technology SLM*. ETH-Zürich, 2014.

[39] Hengfeng Gu, Haijun Gong, Deepankar Pal, Khalid Rafi, Thomas Starr, and Brent Stucker. Influences of energy density on porosity and microstructure of selective laser melted 17-4PH stainless steel. In *Proceedings of the Solid Freeform Fabrication Symposium*, pages 474–489, Austin, TX, 2013.

[40] M. Averyanova and Ph. Bertrand. Direct manufacturing of dense parts from martensitic precipitation hardening steel gas atomized powder by selective laser melting (SLM) technology. In *4th International Conference on Advanced Research in Virtual and Rapid Prototyping*, pages 343–348, Leiria, Portugal, October 2009.

[41] David GT Denison. *Bayesian methods for nonlinear classification and regression*, volume 386. John Wiley & Sons, 2002.

[42] Andrew Gelman, John B Carlin, Hal S Stern, and Donald B Rubin. *Bayesian Data Analysis, (Chapman & Hall/CRC Texts in Statistical Science)*. Chapman and Hall/CRC, 2003.

[43] Huiyan Sang and Jianhua Z Huang. A full scale approximation of covariance functions for large spatial data sets. *Journal of the Royal Statistical Society: Series B (Statistical Methodology)*, 74(1):111–132, 2012.

[44] Peter J Green. Reversible jump markov chain monte carlo computation and bayesian model determination. *Biometrika*, 82(4):711–732, 1995.

[45] Peter D Hoff. *A first course in Bayesian statistical methods*. Springer Science & Business Media, 2009.

[46] American Society of Testing Materials. ASTM B962–14: Standard test methods for density of compacted or sintered powder metallurgy (PM) products using archimedes' principle. Standard, ASTM, 2012. [Online]. Available from `http://www.astm.org/Standards/B962.htm`.